ETM+ using railroad valley playa. *IEEE Trans. Geosci. Remote Sensing*, 2003, **41**, 1180–1188.

5. Chander, G., Meyer, D. J. and Helder, D. L., Cross calibration of the Landsat-7 ETM+ and EO-1 ALI sensor. *IEEE Trans. Geosci. Remote Sensing*, 2004, **42**, 2821–2831.

6. Donegan, S. J. and Flynn, L. P., Comparison of the response of the Landsat 7 Enhanced Thematic Mapper Plus and the Earth Observing-1 Advanced Land Imager over active lava flows. *J. Volcanol. Geotherm. Res.*, 2004, **135**, 105–126.

7. Chander, G., Angal, A., Choi, T. and Xiong, X., Radiometric cross-calibration of EO-1 ALI with L7 ETM+ and Terra MODIS sensors using near-simultaneous desert observations. *IEEE J. Sel. Top. Appl. Earth Obs. Remote Sensing*, 2013, **6**, 386–399.

8. Petropoulos, G. P., Kontoes, C. C. and Keramitsoglou, I., Land cover mapping with emphasis to burnt area delineation using co-orbital ALI and Landsat TM imagery. *Int. J. Appl. Earth Obs. Geoinf.*, 2012, **18**, 344–355.

9. Pu, R., Bell, S., Meyer, C., Baggett, L. and Zhao, Y., Mapping and assessing seagrass along the western coast of Florida using Landsat TM and EO-1 ALI/Hyperion imagery. *Estuarine Coastal Shelf Sci.*, 2012, **115**, 234–245.

10. Price, J. C., Calibration of satellite radiometers and the comparison of vegetation indices. *Remote Sensing Environ.*, 1987, **21**, 15–27.

11. Belchansky, G. I. and Douglas, D. C., Integrating remotely sensed data with an ecosystem model to estimate net primary productivity in East Asia. *Remote Sensing Environ.*, 2002, **81**, 58–66.

12. Francis, S, C., Richard, F. and Jing, C., Comparison and evaluation of medium resolution imaging spectrometer leaf area index products across a range of land use. *Remote Sensing Environ.*, 2010, **114**, 950–960.

13. Yu, T. *et al.*, Comparison of the influence factors on NDVI for CCD camera and WFI imager on CBERS-02. *Science China Ser. E (Supp. I)*, 2005, **48**, 100–115.

14. Li, G. *et al.*, Comparison of spectral characteristics between China HJ1-CCD and Landsat 5 TM imagery. *IEEE J. Sel. Top. Appl. Earth Obs. Remote Sensing*, 2013, **6**, 139–148.

15. Fensholt, R., Sandholt, I. and Stisen, S., Evaluating MODIS, MERIS, and VEGETATION vegetation indices using *in situ* measurements in a semiarid environment. *IEEE Trans. Geosci. Remote Sensing*, 2006, **44**, 1774–1786.

16. Chander, G., Markham, B. L. and Helder, D. L., Summary of current radiometric calibration coefficients for Landsat MSS, TM, ETM+, and EO-1 ALI sensors. *Remote Sensing Environ.*, 2009, **113**, 893–903.

Geomorphic evidence of late Quaternary displacement of the Karakoram Fault in Nubra and Shyok valleys, Ladakh Himalaya

Watinaro Imsong[1,3,]*, Falguni Bhattacharya[2], Rajeeb Lochan Mishra[1] and Sarat Phukan[3]

[1]Wadia Institute of Himalayan Geology, Dehradun 248 001, India
[2]Institute of Seismological Research, Gandhi Nagar 382 421, India
[3]Department of Geological Sciences, Gauhati University, Guwahati 781 013, India

The present study ascertains the spatial variability in the extent of activity of the Karakoram Fault (KF) in Nubra and Shyok river valleys (Karakoram), which was known to be active during the Holocene. Towards this we have used conventional morphometric indices supported by geomorphological observations on the pattern of alluvial and bedrock streams, alluvial fan geometry and moraines. The right lateral displacement associated with KF is geomorphologically expressed by the lateral deflections of the bedrock and alluvial streams toward northwest–southeast as they cut across the Fault. Indirect age estimates inferred based on slip rate of KF suggest that the deflection of bedrock streams with prominent shutter ridges is the cumulative expression of activity of KF since the middle Pleistocene, which continued till the late Holocene.

Keywords: Alluvial and bedrock streams, geomorphic evidence, morphometry, right lateral displacement.

THE convergent tectonics of the Himalaya has not changed considerably since the Miocene, and the orogeny manifests a quasi-steady state[1]. The trace of deformational episodes that progressed in space and time can be seen in the sequential evolution of major terrain boundary thrusts[1]. In the northwestern Himalaya, the Indus Suture Zone (ISZ) and Shyok Suture Zone (SSZ) are displaced by the right-lateral Karakoram Fault (KF) system[1–3]. The Shyok and Nubra valleys are intersected by KF, and the southern end of the Fault merges with the Indus (Yarlung) Suture Zone near Mount Kailas[2,4]. Separating the central Karakoram and Ladakh range[5,6], the KF is a NW–SE striking, normal–dextral fault which has displaced the Jurassic–Cretaceous Karakoram batholith from the Gangdese batholith with a displacement of ~1000 km causing the eastward extrusion of the Tibetan Plateau[2,7,8]. According to Searle *et al.*[9–11], although KF is active today, the right lateral offset is probably less than ~120–150 km and the displacement continued since early to mid-Miocene. Studies suggest that KF is undergoing trasnpressional and transtensional tectonics[8,12–14]. According to Searle *et al.*[6], ~150 km right-lateral displacement with a vertical

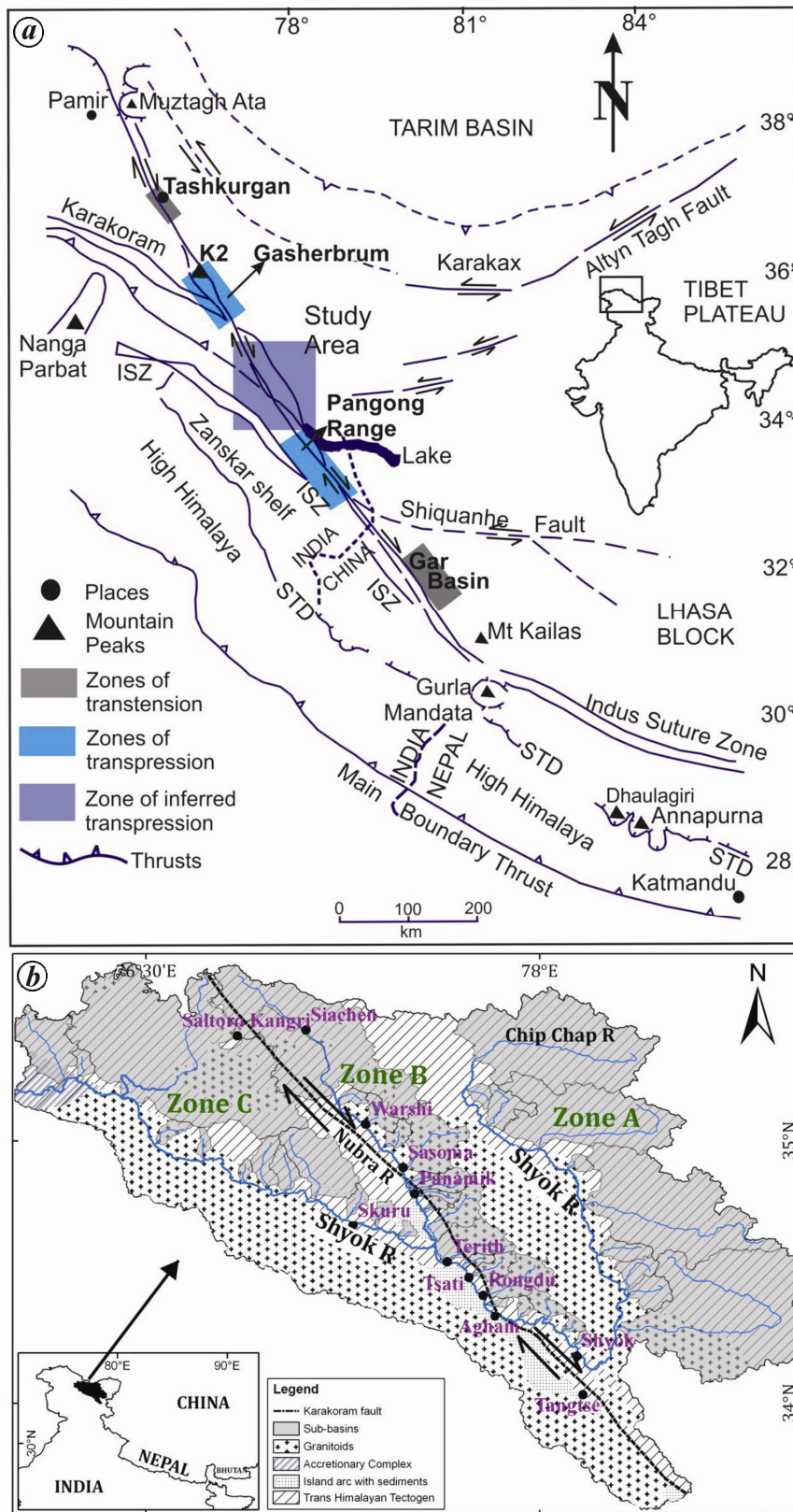*For correspondence. (e-mail: imsongnar@gmail.com)

Figure 1. *a*, Regional map of the Karakoram Fault (KF) zone in NW Himalaya modified after Searle *et al.*[6], showing major zones and structures. ISZ, Indus Suture Zone; STD, South Tibetan Detachment System. *b*, Litho-tectonic map of the study area modified after the Seismotectonic Atlas of India prepared by the Geological Survey of India (2000) showing the trend of KF. Three segments, viz. zone A, zone B and zone C are marked. The shaded (grey) area represents sub-basins selected morphometric analysis in the study area.

exhumation of ~20 km (at 3.0 mm/a) occurred during transpressional tectonics. This was followed by the dextral strike-slip phase along the central part of KF. The transpressionally uplifted mountain ranges and transtensional basins are found distributed along the KF (Figure 1 a)[6,13,14].

Studies based on displaced rocks, alluvial fans and streams, and moraines along the different segments of KF suggest that the Fault has been displaced at the rate of ~8.3, ~4 ± 1 and ~10.7 ± 0.7 mm/year (refs 6, 15, 16). With the advent of GPS, real-time monitoring of KF showed[17] that it is being laterally displaced at ~3.4 ± 5 mm/year, and is in agreement with the earlier observations[15]. Contrary to the above, Robinson[18,19], based on the observation of Quaternary loess, glacial and fluvial deposits in the northern end of the KF system, suggested that there is virtually no movement along the Fault. Majority of the studies mentioned above indicate that KF was active during the Holocene, which is ongoing with an exception of the observation made by Robinson[18,19].

Based on the above, it can be suggested that (i) the KF came into existence during the Miocene[11], probably contemporaneous with the evolution of the Higher Himalaya, and (ii) the activity continued during the Holocene and does so in the recent times as well[15,17]. In the present study, a synoptic view of the activity along KF during the late Quaternary period is presented using conventional morphometric indices and geomorphic evidences obtained from the Nubra and Shyok valleys in Ladakh Himalaya.

Conventional morphometry and its derivatives are used to identify anomalous behaviour of alluvial and bedrock streams, and alluvial fans in the Shyok–Tectonic Zone (between 35.58°N, 75.94°E and 33.52°N, 78.91°E) covering an area of ~31,000 sq. km in the Nubra and Shyok river valleys (Figure 1 b). The timing of the displacement was ascertained using the existing chronology obtained by Brown et al.[15]. Mapping of the south-draining streams which drain into the Shyok and Nubra rivers was carried out using 30 m SRTM–DEM data obtained from http://earthexplorer.usgs.gov/ (Figure 1 b) following 'Horton–Strahler' order[20,21]. As the study area covers varied altitudinal ranges, it has been divided into three zones, viz. zone A (upstream segment) between the Shyok glacier and Shyok village; zone B (middle segment) between Siachen glacier and Shyok village, and zone C (downstream segment) between Skuru in the Shyok valley up to the southwestern slope of Saltoro ridge (Figure 1 b).

Hypsometric analysis is the study of the distribution of ground surface/or horizontal cross-sectional area of a basin with respect to elevation[22]. This method describes the theoretical evolution of a landscape through different stages and is a powerful tool to differentiate tectonically active regions from inactive ones[23]. The hypsometric integral (HI) is the area under the hypsometric curve which relates the percentage of total relief to cumulative percentage area. Pike and Wilson[24] mathematically demonstrated that the elevation–relief ratio E given by Wood and Snell[25] is equivalent to HI. The HI index is calculated as

$$HI = (E_{mean} - E_{min})/(E_{max} - E_{min}),$$

where E_{mean} is the mean elevation value, E_{max} the maximum elevation value and E_{min} is the minimum elevation value (outlet)[22]. The HI value varies from 1.0 to 0.0; HI values ≥0.60 with a convex-up curve indicate young, actively uplifting topography, and HI values ≤0.30 with a sigmoidal-shaped curve indicate a mature stage of development. Willgoose and Hancock[26], however, considered HI values ~0.5 with a more balanced, flattened, s-shaped or straight hypsometric curves to signify relatively stable but still developing landscape.

The HI values were computed for nine sub-basins of zone A, 21 sub-basins of zone B and nine sub-basins of zone C (left flank of Shyok and Nubra rivers). These varied from 0.79 to 0.87 in zone A, 0.70 to 0.86 in zone B and 0.61 to 0.81 in zone C respectively (Table 1). Zone A exhibited slightly higher HI values than zones B and C. The hypsometric curves of all sub-basins showed near straight to marginally convex-up profiles (Figure 2), implying that uplift is outpacing erosion. The insignificant difference in the mean HI values (Table 1), suggests that the Shyok and Nubra river basins are undergoing appreciable uplift/deformation.

Keller and Pinter[23] suggested quantitative estimation of the drainage basin, and corresponding drainage pattern and geometry associated with the tectonically active

Table 1. Hypsometric integrals (HIs) calculated for sub-basins of zones A–C

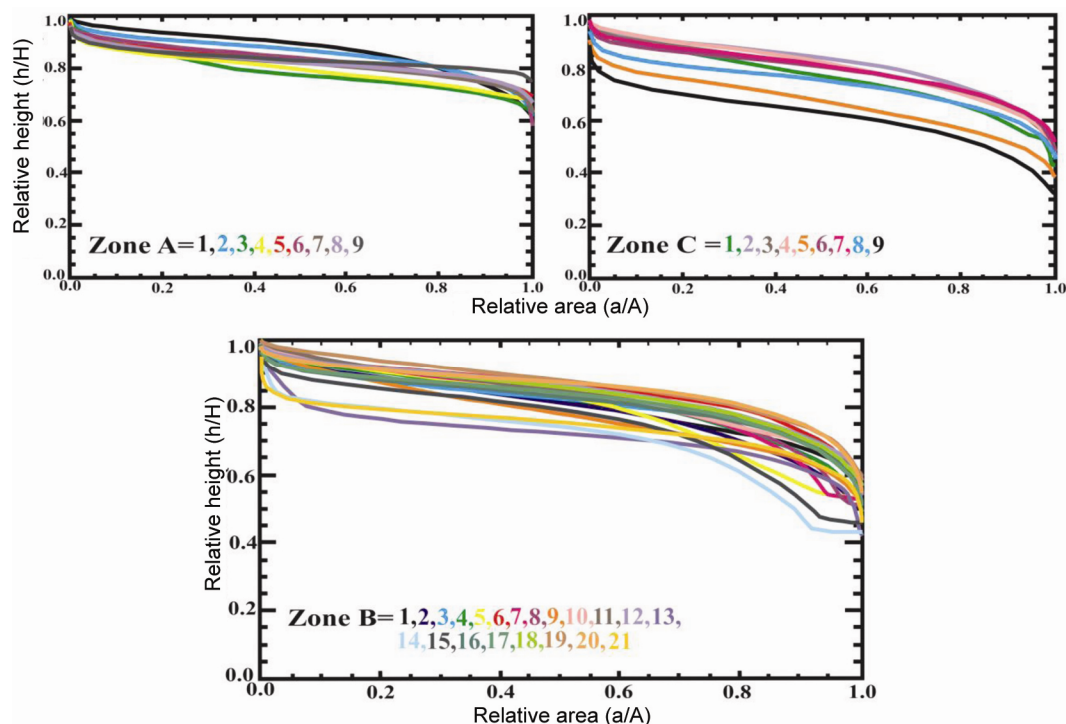| Zone A	HI	Zone B	HI
1	0.87	1	0.81
2	0.85	2	0.79
3	0.79	3	0.81
4	0.79	4	0.82
5	0.83	5	0.79
6	0.83	6	0.85
7	0.81	7	0.81
8	0.82	8	0.82
9	0.83	9	0.78
		10	0.83
Zone C	HI	11	0.83
1	0.76	12	0.84
2	0.81	13	0.71
3	0.79	14	0.70
4	0.80	15	0.75
5	0.66	16	0.81
6	0.78	17	0.82
7	0.79	18	0.84
8	0.72	19	0.86
9	0.61	20	0.85
		21	0.74

Figure 2. Mean percentage hypsometric curves of zones A–C. The almost flattened 'S' curve signifies an active and evolving landscape[26].

Table 2. Asymmetric factor, AF% calculated for the selected sub-basins in zones A–C. Values less than 50% indicate tectonic tilting on the right side of the basin, whereas those greater than 50% indicate tilting on the left side of the basin

Zone A	AF%	Zone B	AF%
1	36	1	45.02
2	39	2	53
3	70	3	49.4
4	53	4	50
5	64	5	33
6	32.5	6	32
7	62	7	58
8	74.7	8	57.6
9	61	9	44
		10	47.5
Zone C	AF%	11	43
1	35	12	20
2	55	13	27
3	37	14	43.5
4	38	15	64.3
5	64	16	37
6	45	17	45.4
7	66	18	35
8	45.5	19	50
9	49.3	20	34
		21	48

terrain. Asymmetric factor (AF) is used to establish tectonic tilting (if any) in a drainage basin and can be calculated as

$$AF = 100(A_r/A_t),$$

where A_r is the area on the right flank of the trunk stream and A_t is the total area of the basin. The value of AF ranges from 0% to 100%. In basins with no tectonic tilting, AF is 50%, whereas values greater or lesser than 50% indicate tectonically induced tilting of the basin.

In zone A, majority of the sub-basins indicated preferential tilt towards the left (southeast), whereas in zones B and C, the sub-basins showed a tilt towards the right (northwest) (Table 2). The preferential tilting of the sub-basins in zones B and C towards the northwest is in accordance with the right lateral displacement of KF.

The stream length (SL) index proposed by Hack[27] is widely used to analyse differences in channel slope, which reflect stream power or competence along a stream profile. SL is defined as

$$SL = (\Delta H/\Delta L)*L,$$

where ΔH is the change in elevation of the reach, ΔL the length of the reach and L is the total channel length from the source to the reach of interest. Keller and Pinter[23] suggested that the SL index is sensitive to changes in channel slope, which in turn is modulated by the rate of bedrock uplift in a near-constant lithology. Thus the anomalously high or low SL index helps in identifying tectonically active and quiescent areas respectively[27].

In the Nubra River, a very high SL gradient peak (SL: 3600) is located in the upstream above Warshi village
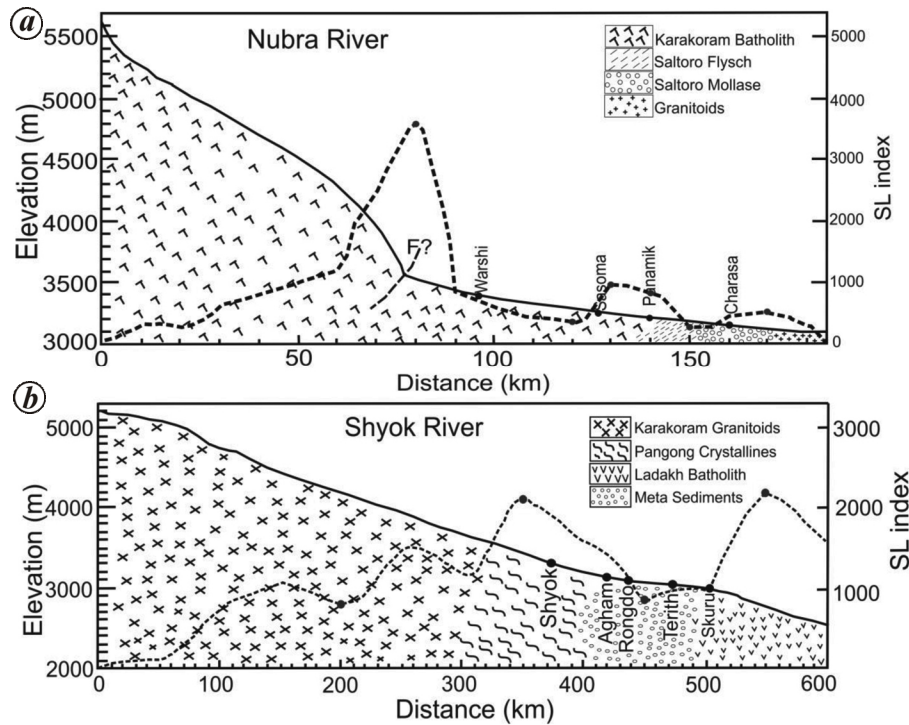
Figure 3. Longitudinal profile of (*a*) Nubra and (*b*) Shyok rivers with stream length (SL) gradient index. The prominent slope break and convex curve in the longitudinal profile of Nubra river may be related to movement along a transverse fault (F?) of the Karakoram Fault. The high and low SL indices at different sections in the Nubra and Shyok rivers indicate recent tectonic activity.

(Figure 3 *a*). Just before Warshi village, a sudden topographic break is observed in the longitudinal profile of the Nubra River; the associated SL peak represents a knick point (Figure 3 *a*). Additionally, two high-gradient peaks are observed between Sasoma (SL: 910) and Panamik (SL: 840) and at downstream of Charasa (SL: 510). However, anomalously low SL values between Warshi and upstream of Sasoma (SL: 360) and between downstream of Panamik and upstream of Charasa (SL: 300; Figure 3 *a*). In the Shyok River, two distinct high gradients in the upstream of Shyok village (SL: 2100) and in the downstream of Skuru village (SL: 2200) are observed. Correspondingly, a very low SL value (SL: 800) is observed upstream of Shyok village (Figure 3 *b*) and between Rongdu and Terith (SL: 900; Figure 3 *b*).

The anomalously low SL values in the central segment of the rivers could be due to the presence of less competent Saltoro molasses and flysh (Figure 3 *a* and *b*). The high stream gradient (Figure 3 *a*) and convex-up curve (prominent slope break) present in the upstream of Nubra River (near Warshi village) do not coincide with any major change in lithology; hence this can be interpreted as an expression of tectonic uplift[28] and suggestive of a subsidiary fault around Warshi village (Figure 4) for the following reasons: In-strike slip settings, localized zones of convergence (transpressional) and divergence (transstensional) movements are observed, which are responsi-

ble for the growth of restraining and releasing bends respectively[29–31]. The higher SL indices (around Warshi village), possibly suggest localized transpressional (convergence) movement. Similar kinematics can be suggested for the very high SL index observed in the Shyok River (Figure 3).

The steepness index (k_s) is used to determine relative estimation on the tectonic instability/stability[32–34]. The longitudinal river profile is governed by a stream-power law relation, according to which the local channel gradient S is a function of the area of its upstream drainage A and can be represented[35] as: $S = k_s A^{-\theta}$, where S is the local channel slope, A the area of upstream drainage at the exit of the channel and θ is the concavity index of the river longitudinal profile. The concavity (θ) and steepness indices (k_s) were estimated using regression analysis of local slope–area data of the streams. Zones undergoing higher surface uplift are associated with relatively higher k_s values.

The channel slope and drainage area were calculated using ~30 m SRTM–DEM data[32]. An assumption that uplift (U) and erosion (K) are uniform was considered in the computation of 12 tributary watersheds and five different segments draining into the main trunk stream of the Shyok River along with the Nubra River watershed (Figure 4)[33]. Separate values of θ have been calculated for each of the streams, which were used to calculate the
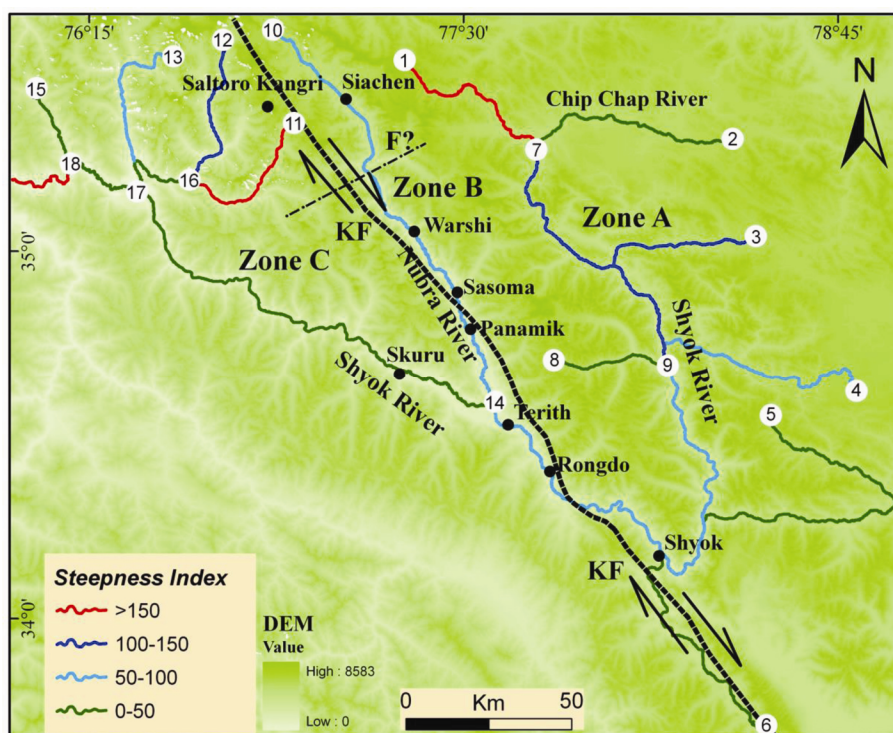
Figure 4. Map of channel steepness index determined for 18 stream segments (white circles). The steepness indices are categorized into four major groups, i.e. very high (>150), high (100–150), moderate (50–100) and low (0–50) values.

Table 3. Steepness data for 18 channels in the Karakoram Fault zone

Sub-basin	θ	k_s
1	0.45	201
2	0.41	40
3	0.42	106
4	0.4	79
5	0.35	21
6	0.32	13
7	0.47	126
8	0.28	10
9	0.44	79
10	0.38	58
11	0.4	151
12	0.39	112
13	0.37	85
14	0.42	40
15	0.34	31
16	0.38	10
17	0.51	23
18	0.55	198

θ, Concavity index; K_s, Steepness index.

steepness indices respectively. The values of concavity index range from 0.28 to 0.55 and steepness index from 10 to 201 (Table 3).

The k_s values obtained were classified under four broad categories, viz. very high (>150), high (100–150), moderate (50–100) and low (0–50). The maximum value was obtained on the headwater end of the Shyok River (segment 1), which is a boundary between the Shyok glacier and the Shyok River ($\theta = 0.45$, $k_s = 201$), whereas the minimum value was obtained in sub-tributary segment 8 ($\theta = 0.28$, $k_s = 10$) and segment 16 ($\theta = 0.38$, $k_s = 10$). We also observed two very high k_s values in sub-tributary segments 11 and 18, and high k_s values in segments 7, 3 and 12. However, moderate k_s values were obtained for the area lying upstream of Shyok village and Terith (segment 9), and between Siachen glacier and Terith (segment 10) (Table 3), which also exhibited concave-up curve profiles along with anomalously high stream gradient (Figure 3 b).

The Shyok and Nubra rivers transport high sediment load due to their proximity to the glaciers and alluvial fans as they lose their ability to incise rapidly due to continuous aggradation. Depending on the timing and amount of sediment supplied, the slopes of a channel may steepen and then relax[36,37]. Therefore, the moderate steepness indices along with concave upward profiles and high stream gradients in segments 9 and 10 suggest the high sediment transport along with the presence of less competent metasediments/mylonitized rocks. Consecutively, the very high and high k_s values which are in agreement with the channel gradient profile (Figure 3 a and b) obtained on the northwestern part of the Shyok basin, suggest more pronounced uplift of the terrain due to the activity of KF and or some subsidiary faults.
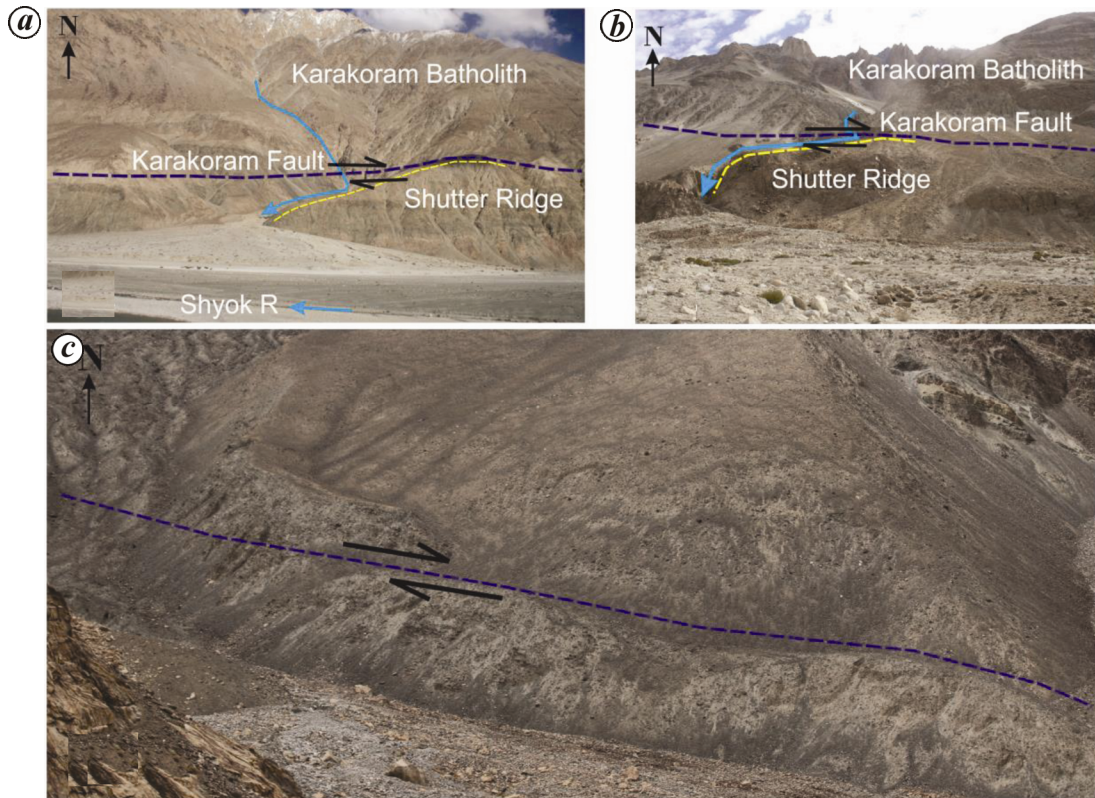
Figure 5. Deflected bedrock streams in (*a*) Rongdo and (*b*) near Sasoma. The second order stream in Rongdo is deflected ~725 m westward with a well-developed shutter ridge. Similarly, near Sasoma the second order stream is displaced ~245 m westward. Both the streams drains south, cutting across the Karakoram batholiths. *c*, The lateral moraine is located on the left flank of Tangtse valley and shows a right lateral displacement of ~5 m.

Previous studies in the Karakoram Range showed that streams respond to movement along the KF; for example, using satellite imageries, Liu[38] observed that moraines in the western shore of Pangong Lake are displaced 300–350 m. Brown *et al.*[15] observed around 45 m right lateral displacement of the stream that drains through alluvial fan/debris flow in the vicinity of KF in Tangtse valley. Here, we present the geomorphic expression of right lateral movement of KF observed in the study area.

The bedrock stream displacement was observed near Rongdo village (Shyok valley) and near Sasoma (Nubra valley). At Rongdo (34.374°N, 77.805°E, elevation 3472 m), the second-order stream having a drainage basin area of 22.3 sq. km had incised ~50 m into the Karakoram batholiths and deflected the river ~725 m westward. The deflected stream has a well-developed shutter ridge (Figure 5 *a*). Similarly, near Sasoma (34.869°N, 77.498°E, elevation 3570 m), the second-order stream had incised ~20 m through the Karakoram batholith and displaced the river ~245 m westward (Figure 5 *b*).

Stream patterns depend on valley slope, tectonic uplift or tilting[23]. The south-draining first- and second-order alluvial streams in the central segment showed distinct westward deflection (Figure 6). The deflected alluvial streams were measured using Google Earth Pro. For

example, near Agham village, two second-order streams, viz. AS-1 and AS-2 were deflected ~37 and ~42 m respectively. Similarly, between northwest of Rongdo and Tsati, two (second- and first-order) streams showed variable westward deflection of ~8 (AS 3) and ~14 m (AS 4) respectively. Further east of Tsati village, a first-order stream (AS5) was deflected ~17 m westward. In addition, on the opposite flank of Charasa and above Warshi (Nubra valley), a westward displacement of two alluvial streams of ~43 (AS 6) and ~32 m (AS 7) was observed (Figure 6).

The alluvial fans emanate from the southward-draining first- or second-order streams and cut across the KF (zone B; Figure 7). Alluvial fans are usually symmetrical half-cones with topographic contours on the surface defining concentric semicircles. However, contours on the surface of the tectonically tilted fans simulate segments of ellipses with their long axes oriented parallel to the direction of tilting; hence the intersection of a tilted cone with a horizontal plane form an ellipse[39]. The amount of tilt can be calculated by fitting ideal ellipses to the contours across the fan and measuring the length of the major and minor axes[32]. Figure 7 *a* represents a generic model of a tilted cone (in map view); Figure 7 *b* and *c* are the cross-sections, fine lines representing topographic contours.
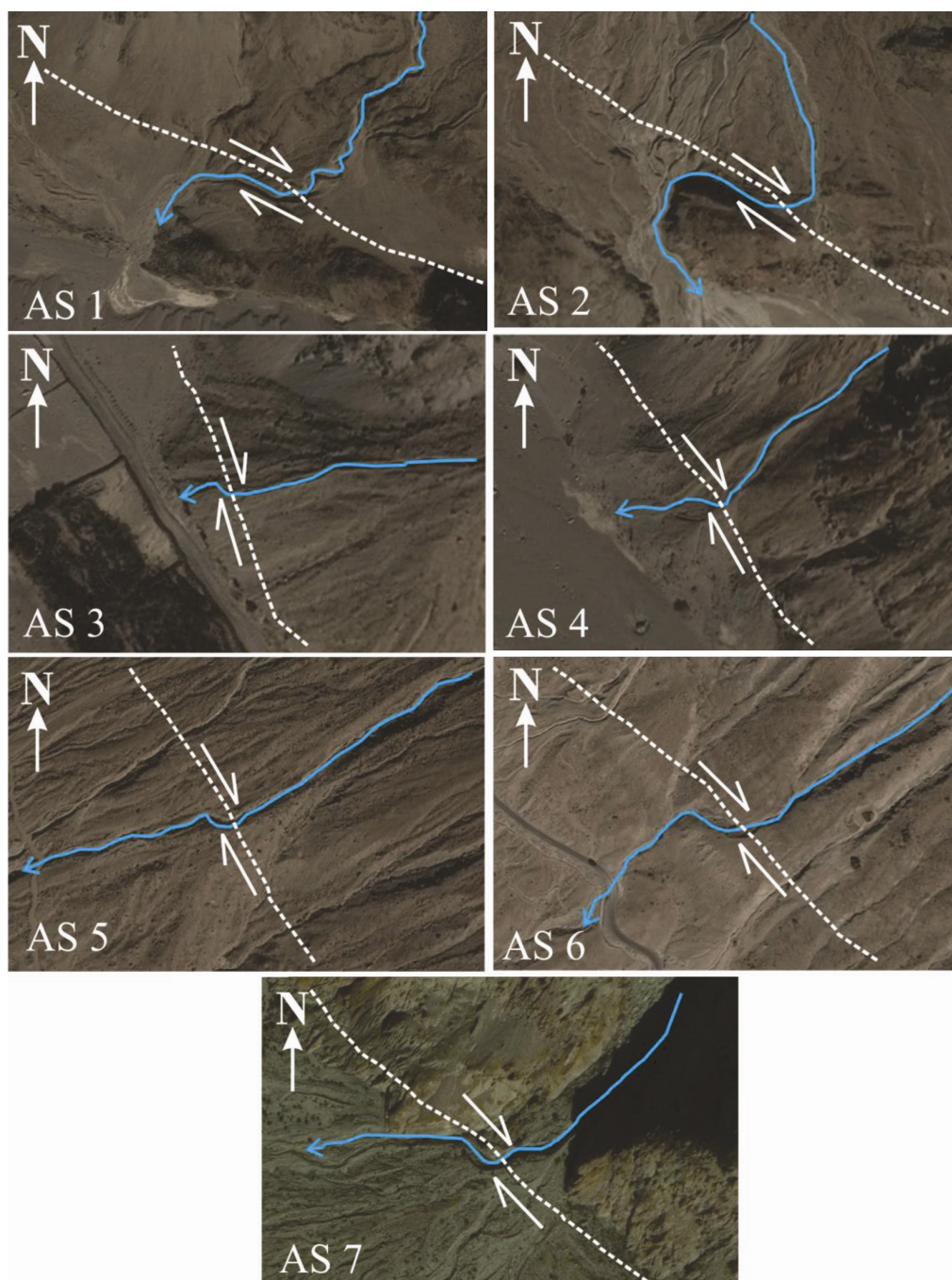
Figure 6. Deflection of young alluvial streams in the study area that flow through alluvial fans and glacial deposits observed using Google Earth images: AS 1 and AS 2 (northeast of Agham village), AS 3 and AS 4 (northwest of Rongdo), AS 5 (east of Tsati village), AS 6 and AS 7 (upstream of Nubra, near Warshi). Note the streams are deflected northwest, which is sympathetic to right lateral displacement associated with the KF.

The angle of tilt (β) of the alluvial fans was calculated using the following equation

$$\beta = \arccos[\{(b/a)^2\sin^2\alpha + \cos^2\alpha\}^{1/2}],$$

where α is the original depositional slope, derived from the slope along the minor axis of the ellipse, b half of the length of the minor axis of the ellipse, and a is half of the length of the major axis of the ellipse. This methodology assumes negligible active deposition, which upon annealing of the fan surface might restore the concentric untilted conical geometry[40].

The 20 alluvial fans were randomly analysed from zone B (Nubra and Shyok valleys), which cut across the NW–SE trending KF (Figure 1). Sediment texture, size, vegetation cover and geomorphic hierarchy allowed us to
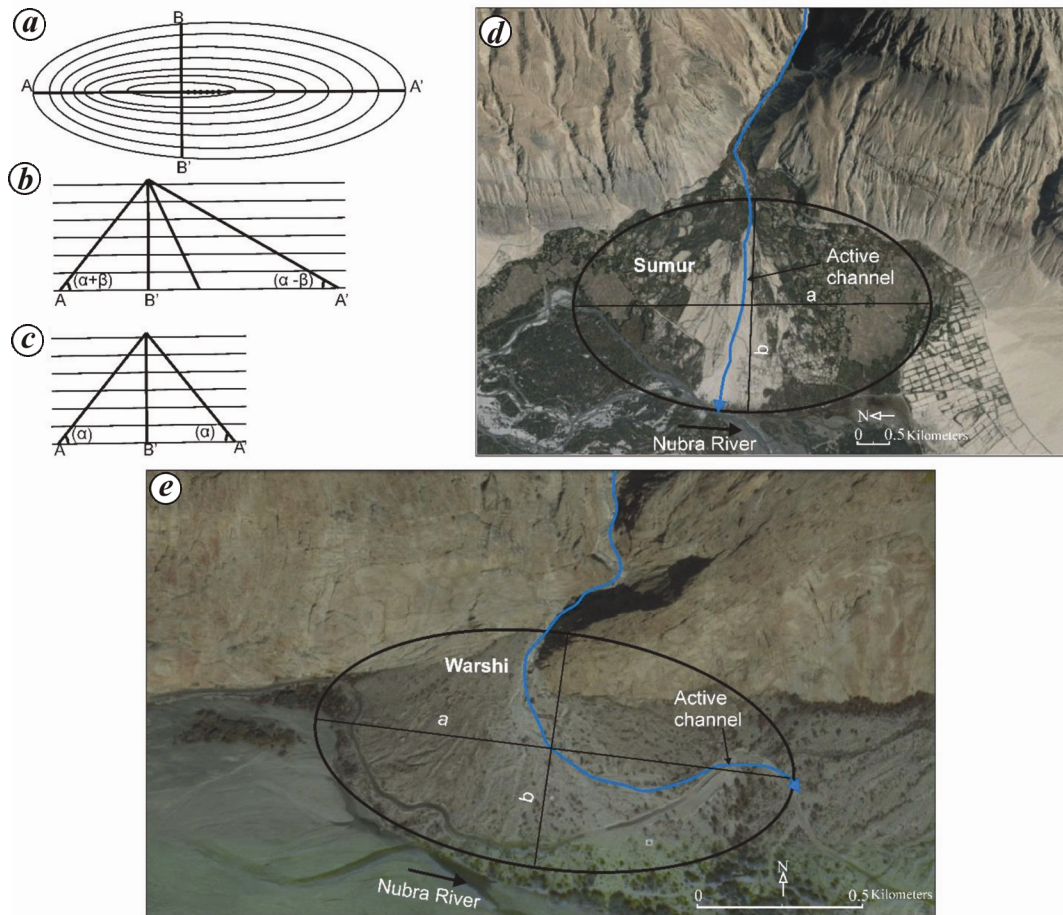
Figure 7. *a*, Generic model on a cone. *b*, *c*, Cross-sections taken across A and A′. *d*, A younger alluvial fan at Warshi with the best-fitted ellipse. *e*, An older alluvial fan at Sumur with an active channel at the middle of the ellipse.

differentiate the younger (vegetation free) and older (vegetation covered) alluvial fans. Around Terith (Nubra valley) alluvial fans had incised the moraine dated to ~18 ka, whereas in the Tangtse valley they cut across the fluvial gravel dated to 11 ka (ref. 41). Among 20 alluvial fans studied, 7 around Warshi village (mostly younger) showed tilt angle varying from 0.16° to 0.39° towards SSE, whereas at Sasoma (east of Warshi), the older fan showed a tilt of ~0.10° towards SSE. Further ~30 km east between Sumur and Tsati villages, the older fans had a tilt of ~0.08° towards west and the younger fans had relatively higher tilt, which varied between 0.10° and 0.39° towards SSE. Similar observations were made in a few selected alluvial fans in the Shyok valley around Rongdo. Figure 7 *d* shows a typical example of the alluvial fan observed in the study area. Note that the active channel in the younger alluvial fan is preferentially tilted towards SSE, whereas in case of the older alluvial fan, the alluvial fan channel is more towards the middle of the ellipse (Figure 7 *e*).

A lateral moraine located on the left flank of Tangtse valley at around 4 km from the Tangtse village (34.07°N, 78.24°E) showed a right lateral displacement of ~5 m

(Figure 5 *c*). This location is in the proximity of the stream displacement[15]. Considering that the valley was aggraded by the early Holocene flood dated to ~11 ka (ref. 41), the displaced moraines could be younger than 11 ka, implying that the displacement postdates early Holocene.

Although the KF is regionally a strike-slip fault, studies suggest it has an oblique slip movement as well, which is responsible for differential uplift along the fault zone[4,10]. Hypsometric analysis indicates high rates of uplift in zone A. Correspondingly, the asymmetric factor indicates that zone B is undergoing preferential right lateral displacement along with appreciable uplift. For example, AF indicates that the sub basins in zones B and C show tilting towards the right. The KF passes through zone B, whereas zone C lies along the Shyok suture and joins the Fault near Terith[42]. The relatively low SL values (in zone B) in the central segment of Shyok and Nubra rivers are ascribed to pulverized lithology (mylonites). However, the sudden break in the river profile and rise in SL index in areas dominated by Karakoram batholiths (homogeneous lithology) in Nubra River valley (above Warshi village), can be attributed to the activity along an

Table 4. Bedrock and alluvial channels that display northwest deflection in the Shyok and Nubra river valleys for which tentative (infered) timing of initiation for deflection has been calculated

Channels	Amount of right lateral deflection (m)	Tentative timing of deflection (ka) assuming slip rate of 4 mm/year[15]
Bedrock channels		
Rongdo ridge channel	~725	180
Sasoma ridge channel	~245	60
Alluvial channels		
AS 1	~37	9
AS 2	~42	10
AS 3	~8	2
AS 4	~14	3.5
AS 5	~17	4
AS 6	~43	10.8
AS 7	~32	8

inferred transverse fault over a transpressional zone of the KF. The k_s values in the western part of zone B and southern slope of Saltoro ridge are high (Figure 4). Contrary to this, in the Shyok River (eastern part of zone B) the low k_s values could be due to the presence of less competent metasedimentary lithology (Figure 1). Summarizing the morphometric evidences, such as very high HI, high peaks of SL and very high k_s values, these can be ascribed to the uplift associated with the transpressional activity of KF. The unambiguous evidence of the activity along KF is manifested by the presence of shutter ridges flanked by abrupt westward-deflected, southward-draining bedrock stream (Figure 5 a and b), deflected alluvial streams (Figure 6), westward tilting of alluvial fan (Figure 7), and lateral displacement in the moraines (Figure 5 c). These evidences provide an additional support to the earlier suggestion that KF is an active structure[10,15,16].

According to Searle[10], geological evidences are virtually non-existent to suggest any large-scale pre-Holocene offsets associated with the KF which, according to him, imply that KF cannot have accommodated major eastward lateral motion of the Tibetan crust. In an earlier study, slip rate estimation assumed that the displaced geomorphic features were either associated with the Last Glacial Maximum (LGM) or early Holocene deglaciation[10]. As a result, variable estimates obtained on the magnitude of displacement, and the antiquity of KF were subjected to large uncertainty[7,10,43]. For example, according to Searle[10], the 32 mm/year slip rate suggested by Avouac and Tapponnier[44] accounts well for the amount of extrusion (<200 km) along KF. On the contrary, the displacement along KF by Brown et al.[15] based on the dating of displaced stream alluvium in Tangtse valley is estimated to be ±4 mm/year and is in accordance with GPS data[17].

The tentative chronology for the initiation of displacement along the bedrock and alluvial streams was assigned using 4 mm/year slip rate obtained by Brown et al.[15]. Based on this, the timing of stream deflection was calculated (Table 4). The results obtained suggest that the bedrock stream deflection was initiated during ~180 and 60 ka respectively, whereas the alluvial stream deflection is dated between early Holocene (~10 ka) and late Holocene (~2 ka), implying continued activity along KF, at least since the late Quaternary till the late Holocene.

The present study, although preliminary in nature, indicates that the activity along KF is an ongoing process which continued through late Holocene. The oldest preserved record of right lateral displacement is geomorphologically expressed by the presence of well-developed shutter ridges in the bedrock stream that probably initiated around 180 and 60 ka. The younger alluvial stream displacement is associated with early to late Holocene activity along KF. Our data based on high HI, tilted sub-basins and varying k_s values in different segments suggest that along with the lateral displacement there is considerable vertical component involved along KF.

1. Hodges, K. V., Tectonics of the Himalaya and southern Tibet from two perspectives. *GSA Bull.*, 2000, **112**(3), 324–350.
2. Peltzer, G. and Tapponnier, P., Formation and evolution of strike-slip faults, rifts and basins during the India – Asia collision: an experimental approach. *J. Geophys. Res.*, 1988, **93**(B12), 15085–15117.
3. Searle, M. P., *Geology and Tectonics of the Karakoram Mountains*, Wiley, Chichester, UK, 1991.
4. Lacassin, R. *et al.*, Large scale geometry, offset and kinematic evolution of the Karakoram fault, Tibet. *Earth Planet. Sci. Lett.*, 2004, **219**, 255–269.
5. Dortch, J. M., Owen, L. A. and Caffee, M. W., Quaternary glaciation in the Nubra and Shyok valley confluence, northernmost Ladakh, India. *Quaternary Res.*, 2010, **74**, 132–144.
6. Searle, M. P., Weinberg, R. F. and Dunlap, W. J., Transpressional tectonics along the Karakoram fault zone, northern Ladakh: constraints on Tibetan extrusion. In *Continental Transpressional and Transtensional Tectonics* (eds Holdsworth, R. E., Strachan, R. A. and Dewey, J. F.), Geological Society of London. Special Publication, 1998, vol. 135, pp. 307–326.
7. Molnar, P. and Tapponnier, P., Cenozoic tectonics of Asia: effects of a continental collision. *Science*, 1975, **189**(4201), 419–426.
8. Matte, Ph. *et al.*, Tectonics of western Tibet between the Tarim and the Indus. *Earth Planet. Sci. Lett.*, 1996, **142**, 311–330.
9. Searle, M. P., Rex, A. J., Tirrul, R., Rex, D. C., Barnicoat, A. and Windley, B. F., Metamorphic, magmatic and tectonic evolution of

the central Karakoram in the Biafo-Baltoro-Hushe regions of North Pakistan. *Geol. Soc. Am., Spec. Pap.*, 1989, **232**, 47–73.

10. Searle, M. P., Geological evidence against large-scale pre-Holocene offstes along the Karakoram fault: Implications for the limited extrusion of the Tibetan Plateau. *Tectonics*, 1996, **15**(1), 171–186.

11. Searle, M. P., Parrish, R. R., Thow, A. V., Noble, S. R., Phillips, R. J. and Waters, D. J., Anatomy, age and evolution of a collision mountain belt: the Baltoro granite batholiths and Karakoram metamorphic complex, Pakistan Karakoram. *J. Geol. Soc. London*, 2010, **167**, 183–202.

12. Brunel, M., Arnaud, N., Tapponnier, P., Pan, Y. and Wang, Y., Kongur Shang Normal Fault: type example of mountain building assisted by extension, Karakoram Fault, Eastern Pamir. *Geology*, 1994, **22**, 707–710.

13. Chevalier, M. L. *et al.*, Fast slip-rate along the northern end of the Karakorum fault system, western Tibet. *Geophys. Res. Lett.*, 2011, **38**(22).

14. Chevalier, M. L., Tapponnier, P., Van der Woerd, J., Ryerson, F. J., Finkel, R. C. and Li, H., Spatially constant slip rate along the southern segment of the Karakorum fault since 200 ka. *Tectonophysics*, 2012, **530**, 52–179.

15. Brown, E. T., Bendick, R., Bourles, D. L., Gaur, V., Molnar, P., Raisbeck, G. M. and Yiou, F., Slip rates of the Karakoram fault, Ladakh, India, determined using cosmic ray exposure dating of debris flows and moraines. *J. Geophys. Res.*, 2002, **107**(B9), 2192.

16. Chevalier, M. L., Ryerson, F. J., Tapponnier, P., Finkel, R. C., Van Der Woerd, J., Li, H. and Qing, L., Slip-rate measurements on the Karakoram fault may imply secular variations in fault motion. *Science*, 2005, **307**, 411–414.

17. Jade, S. *et al.*, GPS measurements from the Ladakh Himalaya, India: preliminary tests of plate-like or continuous deformation in Tibet. *GSA Bull.*, 2004, **116**, 1385–1391.

18. Robinson, A. C., Geological offsets across the northern Karakoram fault: implications for its role and terrane correlations in the western Himalayan–Tibetan orogen. *Earth Planet. Sci. Lett.*, 2009, **279**, 123–130.

19. Robinson, A. C., Evidence against Quaternary slip on the northern Karakoram fault suggests kinematic reorganization at the western end of the Himalayan–Tibetan orogen. *Earth Planet. Sci. Lett.*, 2009, **286**, 158–170.

20. Horton, R. E., Erosional development of streams and their drainage basins: hydrophysical approach to quantitative morphology. *GSA Bull.*, 1945, **56**, 275–370.

21. Strahler, A. N., Quantitative analysis of watershed geomorphology. *Am. Geophys. Union*, 1957, **38**(6), 913–921.

22. Strahler, A. N., Hypsometric (area–altitude) analysis of erosional topography. *Geol. Soc. Am. Bull.*, 1952, **63**, 1117–1142.

23. Keller, E. A. and Pinter, N., *Active Tectonics: Earthquake, Uplift, and Landscape*, Prentice Hall, Englewood Cliffs, USA, 2002, 2nd edn, pp. 121–147.

24. Pike, R. J. and Wilson, S. E., Elevation–relief ratio, hypsometric integral and geomorphic area–altitude analysis. *Geol. Soc. Am. Bull.*, 1971, **82**, 1079–1084.

25. Wood, W. F. and Snell, J. B., A quantitative system for classifying landforms (No. TR-EP-124). Quartermaster Research and Engineering Command Natick MA, 1960.

26. Willgoose, G. and Hancock, G., Revisiting the hypsometric curve as an indicator of form and process in transport-limited catchment. *Earth Surf. Process Landforms*, 1998, **23**, 611–623.

27. Hack, J. T., Stream profile analysis and stream gradient index. *J. Res. US Geol. Surv.*, 1973, **1**(4), 421–429.

28. Whittaker, A. C., Cowie, P. A., Attal, M., Tucker, G. E. and Roberts, G. P., Bedrock channel adjustment to tectonic forcing: implications for predicting river incision rates. *Geology*, 2007, **35**(2), 103–106.

29. Crowell, J. C., Sedimentation along the San Andreas fault, California. In *Modern and Ancient Geosynclinal Sedimentation* (eds Dott, R. H and Shaver, R. H.), SEPM Special Publications, 1974, vol. 19, pp. 292–303.

30. Christie-Blick, N. and Biddle, K. T., Deformation and basin formation along strike-slip faults. In *Strike-Slip Deformation, Basin Formation, and Sedimentation* (eds Biddle, K. T. and Christie-Blick, N.), SEPM Special Publications, USA, 1985, vol. 37, pp. 1–34.

31. Cunningham, W. D. and Mann, P., *Tectonics of Strike-Slip Restraining and Releasing Bends*, Geological Society of American Bulletin, Special Publication, London, USA, 2007, vol. 290(1), pp. 1–12.

32. Snyder, N. P., Whipple, K. X., Tucker, E. and Merritts, D. J., Landscape response to tectonic forcing: digital elevation model analysis of stream profiles in the Medocino triple junction region, northern California. *GSA Bull.*, 2000, **112**(8), 1250–1263.

33. Kirby, E. and Whipple, K. X., Quantifying differential rock-uplift rates via stream profile analysis. *Geol. Soc. Am. Bull.*, 2001, **29**(5), 415–418.

34. Kirby, E., Whipple, K. X., Tang, W. and Chen, Z., Distribution of active rock uplift along the eastern margin of the Tibetan Plateau: inferences from bedrock channel longitudinal profiles. *J. Geophys. Res.*, 2003, **108**(B4), 2217.

35. Hack, J. T., Studies of longitudinal stream profiles in Virginia and Maryland. *US Geol. Surv. Prof.*, 1957, **294**(B), 45–97.

36. Sklar, L. S. and Dietrich, W. E., A mechanistic model for river incision into bedrock by saltating bed load. *Water Resour. Res.*, 2004, **40**, W06301.

37. Gasparini, N. M., Bras, L. R. and Whipple, K. X., Numerical modelling of non-steady state river profile evolution using a sediment flux dependent incision model. In *Tectonics, Climate and Landscape Evolution* (eds Willet, S. D. *et al.*), Geological Society of America Special Paper, 2006, vol. 398, pp. 127–141.

38. Liu, Q., Ph D thesis, Université Paris VII, 1993.

39. Pinter, N. and Keller, E. A., Late-Quaternary deformation in northern Owens Valley, California: geomorphic analysis of tectonic tilt. *Geol. Rundsch.*, 1995, **84**, 200–212.

40. Burbank, D. W. and Anderson, R. S., *Tectonic Geomorphology*, Blackwell Science Oxford, 2001, p. 270.

41. Dortch, J. M., Owen, L. A., Caffee, M. W. and Kamp, U., Catastrophic partial drainage of Pangong Tso, northern India and Tibet. *Geomorphology*, 2011, **125**, 109–121.

42. Searle, M. P., *Colliding Continents: A Geological Exploration of the Himalaya, Karakoram and Tibet*, Oxford University Press, Oxford, UK, 2013, p. 433.

43. Liu, Q., Avouac, J. P., Tapponnier, P. and Zhang, Q., Holocene movement along the southern part of the Karakorum Fault: In International Symposium on the Karakorum and Kunlun Mountains, Kashi [*sic*], China, 5–9 June 1992, p. 91.

44. Avouac, J. P. and Tapponnier, P., Kinematic model of active deformation in central Asia. *Geophys. Res. Lett.*, 1993, **20**(10), 895–898.